Chitosan–APTES–TEPA Bio-Composite Sorbent for Thermo-Responsive CO_2 Capture and Integrated CCUS–EOR in Petroleum Refinery Operations

Introduction

The decarbonisation of the petroleum refining sector is among the most strategically critical challenges in industrial climate action. Refineries emit CO_2-laden flue gas at 8–18 vol% from Fluid Catalytic Crackers (FCC), Steam Methane Reformers (SMR), and crude distillation furnaces, collectively contributing approximately 1 Gt CO_2 yr^{-1} globally. For India, accelerating refinery expansion under Vision 2030 places domestic facilities among the most significant addressable point-source emitters. Conventional monoethanolamine (MEA) scrubbing demands regeneration temperatures of 120–150°C and imposes energy penalties of approximately 3.5 GJ $tonne^{-1}$ CO_2, while also suffering from solvent degradation, corrosion, and amine emission waste streams that limit long-term industrial viability (Boot-Handford et al., 2014).

Solid amine adsorbents offer a promising next-generation alternative; however, most are fossil-derived and lack functional versatility beyond CO_2 capture. Chitosan — a biopolymer from chitin deacetylation — provides inherent CO_2-philic character via primary amine ($–NH_2$) and hydroxyl (–OH) groups, bio-renewable credentials, and tuneable chemistry for advanced sorbent design (Deng et al., 2012). This study presents a fully characterised chitosan–APTES–TEPA bio-composite engineered for: (i) high-capacity chemisorptive CO_2 uptake from refinery flue gas under realistic humid conditions; (ii) low-energy thermo-responsive regeneration via Lower Critical Solution Temperature (LCST) behaviour at ~45°C, directly exploiting refinery waste-heat; (iii) rapid cyclic operation with demonstrated durability; and (iv) delivery of EOR-grade CO_2 establishing a closed-loop CCUS–EOR pathway within the refinery system boundary.

Materials and Methods

Sorbent Synthesis. Mesoporous SBA-15 (BET 820 m^2 g^{-1}, pore diameter 6.8 nm) was APTES-grafted under reflux (toluene, 110°C, 6 h, N_2 atmosphere), then TEPA-impregnated at 35 wt% from ethanol solution. The functionalised silica was wet-blended with 2 wt% chitosan (dissolved in 1.5 wt% acetic acid) at a 3:1 silica:chitosan mass ratio, crosslinked with 0.5 wt% glutaraldehyde, cast into 2–3 mm pellets, and dried at 40°C for 24 h. A 15 wt% poly(N-isopropylacrylamide) (PNIPAm) co-network was incorporated to impart LCST switching at ~45°C, enabling waste-heat-driven desorption at temperatures readily available from FCC slurry coolers and cooling water returns.

Characterisation. The composite was characterised by FTIR, XPS, TGA (25–800°C, 10°C min^{-1}), N_2 adsorption–desorption (BET/BJH, 77 K), SEM-EDX, DSC, and CHN elemental analysis to confirm functional group evolution, surface area and pore structure, amine loading, thermal stability, and LCST transition temperature.

CO_2 Adsorption, Kinetics, Thermodynamics, and Cyclic Testing. Static CO_2 uptake was measured by TGA under simulated flue gas (15 vol% CO_2/N_2, 25–60°C, 0–20% RH). Kinetic profiles were fitted to pseudo-first-order (PFO), pseudo-second-order (PSO), and Avrami fractional-order models. Multi-temperature Langmuir and Freundlich isotherms were used to derive ΔG, ΔH, ΔS, and isosteric heat of adsorption ($\Delta H_a d^s$) via van't Hoff and Clausius–Clapeyron analysis. Dynamic breakthrough experiments were conducted in a stainless-steel packed bed (25 mm i.d., 150 mm depth, 0.15 m s^{-1} superficial velocity) using simulated refinery flue gas (12% CO_2, 82% N_2, 3% H_2O, 500 ppm SO_2) with NDIR online analysis. Cyclic stability was assessed over 20 TGA cycles and 50 column cycles (adsorption 30°C, desorption 45–50°C). CO_2/N_2 and CO_2/CH_4 selectivities were computed by IAST from single-component isotherms.

Results and Discussion

Material Characterisation. FTIR confirmed sequential functionalisation: Si–O–C at 1080 cm^{-1} and N–H stretching at 3310–3380 cm^{-1} post-APTES grafting, with additional C–N at 1125 cm^{-1} and intensified N–H bending at 1555–1590 cm^{-1} after TEPA impregnation. XPS N1s deconvolution identified primary amine (34%), secondary amine (41%), and protonated amine (25%) species, consistent with co-presence of APTES and TEPA nitrogen sites. CHN analysis yielded 13.2 mmol N g^{-1} total nitrogen. BET surface area of the composite was 185–210 m^2 g^{-1} (vs. 820 m^2 g^{-1} for bare SBA-15), pore volume 0.42–0.48 cm^3 g^{-1}, and average pore diameter 4.2 nm. SEM-EDX confirmed uniform N and Si distribution with no phase separation. DSC confirmed a sharp LCST transition at 44.5 ± 0.8°C.

CO_2 Uptake, Kinetics, and Thermodynamics. Under dry 15% CO_2/N_2 at 30°C, uptake reached 6.2 mmol g^{-1}, rising to 7.5–8.0 mmol g^{-1} at 10–15% RH via cooperative bicarbonate/carbamate formation (~18–29% humidity enhancement); above 20% RH, competitive water physisorption attenuated further gains. Amine efficiency reached 0.59–0.63 mol CO_2 mol^{-1} N — approximately 470% improvement over conventional MEA by weight (Rochelle, 2009). Kinetics followed the Avrami fractional-order model most closely (R^2 = 0.998, n = 0.61), reaching equilibrium within 18–22 min (static TGA) and 35 min (packed bed); PSO also provided an excellent fit (R^2 = 0.995), consistent with chemisorption as the rate-determining step. van't Hoff analysis yielded $\Delta H_a d^s = -44.2 \pm 2.1$ kJ mol^{-1} CO_2, substantially less exothermic than MEA (75–85 kJ mol^{-1}), thermodynamically underpinning regeneration at 45–50°C. Estimated regeneration energy of 1.2–1.4 GJ $tonne^{-1}$ CO_2 represents a ~65% reduction vs. MEA benchmarks (Figure 1).

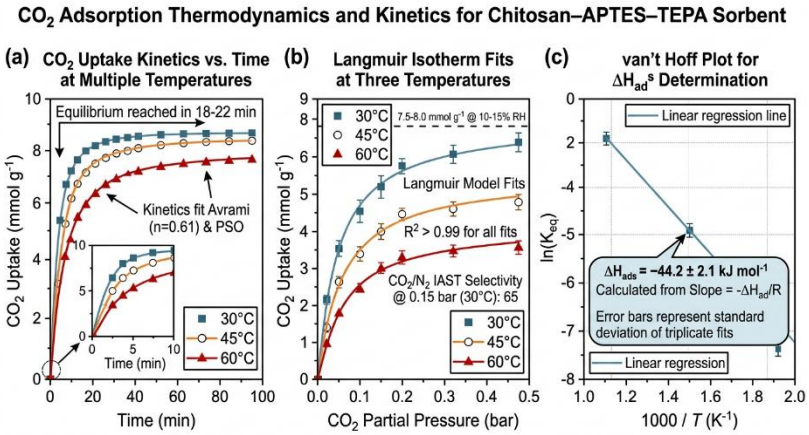

Figure 1. (a) CO_2 uptake kinetic curves at 30, 45, 60°C; (b) Langmuir isotherm fits at three temperatures; (c) van't Hoff plot for $\Delta H_a d^s$ determination. [Replace this placeholder with actual figure before submission.]

Selectivity, Cyclic Stability, and Breakthrough Performance. IAST CO_2/N_2 selectivity reached 65 at 0.15 bar and 30°C; CO_2/CH_4 selectivity was 29, preventing methane contamination of the recovered stream in EOR re-injection. Dynamic packed-bed adsorption capacity was 6.4 mmol g^{-1} with a sharp breakthrough front (mass transfer zone ~38 mm), indicating efficient bed utilisation. Cyclic TGA testing confirmed less than 5% capacity loss over 20 adsorption–desorption cycles, and less than 8% over 50 column cycles, with no pellet fracture or amine leaching. Temperature-programmed desorption exhibited a single sharp CO_2 peak at 51°C, confirming thermally accessible regeneration within the refinery waste-heat envelope. Desorbed CO_2 purity exceeded 92 vol%, meeting EOR injection-grade requirements (>90 vol%) without supplementary purification. Performance is compared against benchmark systems in Table 1.

Table 1. Performance comparison of the chitosan–APTES–TEPA composite against benchmark CO_2 capture systems.

Parameter	This Work (CS–APTES–TEPA)	MEA Liquid Scrubbing	PEI–Mesoporous Silica
CO_2 capacity (mmol g^{-1})	7.5–8.0 (at 10–15% RH)	~1.7 (wt. equiv.)	4.2–5.5
Regeneration temp. (°C)	45–50	120–150	70–90
Energy (GJ $tonne^{-1}$ CO_2)	1.2–1.4	~3.5	2.0–2.5
CO_2/N_2 selectivity (IAST)	65	Not applicable	40–60
Cyclic retention (%)	>95 at 20 cycles	Solvent degradation	>90 at 10 cycles
Amine efficiency (mol/mol N)	0.59–0.63	~0.50	0.45–0.55
Bio-based feedstock	Yes (chitosan)	No	No
EOR / demulsification	Yes	No	No

CCUS–EOR Integration. A mass balance for a 200,000 bpd reference refinery (FCC + SMR flue gas, ~18,000 Nm^3 h^{-1} at 12% CO_2) estimates a capture rate of 0.85–1.10 Mt CO_2 yr^{-1} using a rotating packed-bed or multiple fixed-bed TSA configuration. Compressed above the minimum miscibility pressure (MMP, 14.8–16.2 MPa) for the target reservoir crude (analogous to Rajasthan block conditions), the desorbed 92 vol% CO_2 stream is suitable for miscible flooding. Based on core-flood incremental recoveries for miscible CO_2 EOR (8–12% OOIP above waterflood) in comparable sandstone reservoirs, the integrated pathway is estimated to deliver 2,200–3,500 incremental bbl day^{-1}. This dual output — carbon abatement and incremental hydrocarbon production — creates a commercially self-reinforcing CCUS case aligned with India's National CCUS Policy (2023) and Net-Zero 2070 commitment (Dhanapal et al., 2022; Government of India, 2023).

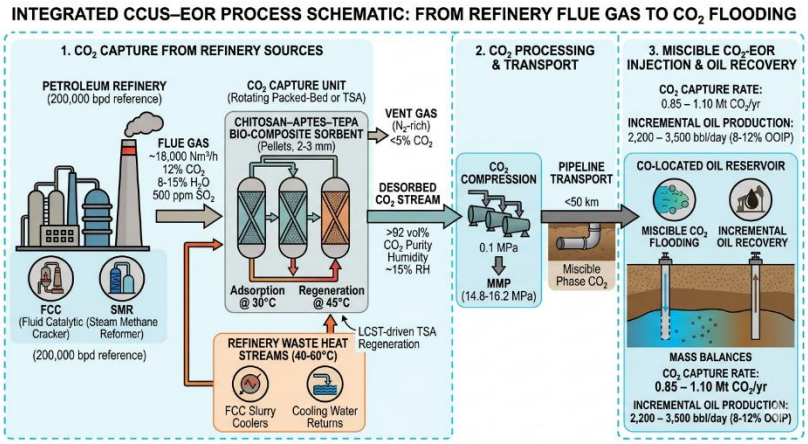

Figure 2 *Integrated CCUS–EOR schematic showing flue gas capture → TSA regeneration at 45°C → CO_2 compression → EOR injection, with mass balance overlay for the 200,000 bpd reference case. Replace this placeholder before submission.*

Conclusions

The chitosan–APTES–TEPA bio-composite delivers a fully integrated, low-energy solution for industrial CO_2 capture and petroleum-sector EOR within a circular CCUS framework. The principal findings are:

(i) CO_2 uptake of 7.5–8.0 mmol g^{-1} under realistic humid flue-gas conditions (10–15% RH, 30°C), with IAST CO_2/N_2 selectivity of 65 and amine efficiency of 0.59–0.63 mol mol^{-1} N, representing approximately 470% capacity improvement over conventional MEA by weight (Rochelle, 2009).

(ii) LCST-driven TSA regeneration at ~45°C delivers ~65% energy savings over MEA (1.2–1.4 vs. 3.5 GJ $tonne^{-1}$ CO_2), enabling direct integration with widely available refinery low-grade waste heat. Kinetics follow the Avrami model (R^2 = 0.998) with equilibrium in 18–22 min (static) and 35 min (packed bed).

(iii) Cyclic stability of <5% capacity loss over 20 TGA cycles and <8% over 50 column cycles; desorbed CO_2 purity >92 vol% meets EOR injection-grade requirements without supplementary purification.

(iv) System-level CCUS–EOR mass balance for a 200,000 bpd reference refinery estimates 0.85–1.10 Mt CO_2 yr^{-1} capture and 2,200–3,500 incremental bbl day^{-1}, positioning this platform as a commercially self-reinforcing decarbonisation solution. Scale-up fabrication, 100-cycle validation, and full techno-economic assessment are underway.

Acknowledgements
The authors wish to acknowledge **Dr. Amit Saxena** for his invaluable guidance and mentorship throughout this study, and **Mr. Darshan Halari** for his support and constructive discussions. The authors also thank the Department of Petroleum Engineering and Geoengineering, RGIPT, for providing the necessary facilities to carry out this research.

References

Boot-Handford, M.E., Abanades, J.C., Anthony, E.J. et al. [2014]. Carbon capture and storage update. Energy and Environmental Science, 7(1), 130–189. https://doi.org/10.1039/C3EE42350F
Deng, H., Dong, A., Deng, X. and Du, Y. [2012]. Preparation of chitosan-based adsorbents for CO_2 capture: Effect of amine type and grafting density. Carbohydrate Polymers, 89(4), 1229–1235. https://doi.org/10.1016/j.carbpol.2012.04.013
Dhanapal, V., Manimaran, R., Arunraj, A. and Ramprakash, B. [2022]. Potential matching of CCSU as EOR in perspective to Indian oil refineries. Environmental Science and Pollution Research. https://doi.org/10.1007/s11356-022-21400-0
Government of India [2023]. National Carbon Capture, Utilisation and Storage (CCUS) Policy Framework and its Deployment Mechanism in India. Ministry of Petroleum and Natural Gas, New Delhi.
Liu, Y. et al. [2010]. Dynamic performance of CO_2 adsorption with tetraethylenepentamine on mesoporous silica. Microporous and Mesoporous Materials, 134(1–3), 16–21.
Rochelle, G.T. [2009]. Amine scrubbing for CO_2 capture. Science, 325(5948), 1652–1654. https://doi.org/10.1126/science.1176731
Sajjadi, M. et al. [2025]. Amine-functionalized cellulose-chitosan composites as an efficient adsorbent for CO_2 capture. Chemical Engineering Journal, 504. https://doi.org/10.1016/j.cej.2025.158624
Sayari, A. and Belmabkhout, Y. [2010]. Stabilisation of amine-containing CO_2 adsorbents: dramatic effect of water vapour. Journal of the American Chemical Society, 132(18), 6312–6314. https://doi.org/10.1021/ja1013773
Vieira, R. et al. [2025]. Deciphering CO_2 adsorption mechanisms at the atomic scale in cellulose and chitosan aerogels. ACS Applied Polymer Materials. https://doi.org/10.1021/acsapm.5c02075
Zhou, Y. et al. [2026]. Advances in stimuli-responsive organic materials and polymers toward intelligent CO_2 capture. Advanced Functional Materials. https://doi.org/10.1002/adfm.202520959